Journal of New Materials for Electrochemical Systems 21, 233-237 (2018)

Dye-sensitized Solar Cell Utilizing TiO_2-sulphur Composite Photoanode: Influence of Sulphur Content

M.Y.A. Rahman[1,*], S.A.M. Samsuri[2] and A.A. Umar[1]

Address

Received: April 08, 2018, Accepted: July 28, 2018, Available online: December 22, 2018

Abstract: *TiO_2-sulphur composite films have been prepared and employed as photoanode of dye-sensitized solar cell (DSSC). The influence of sulphur content in term of thiourea concentration on the structural and optical properties of the sample has been investigated. The anatase, sulphur and the secondary phase of SO_3 and Ti_3S_4 present in the composite. The 0.3 M sample possesses the highest reflection in visible region. The luminescence peak intensity at 460 nm decreases with thiourea concentration. Raman characterization reveals that the peak at 474 cm^{-1} corresponds to the A_{1g} symmetric stretching mode of sulphur. The effect of the sulphur precursor concentration on the performance parameters of the device has also been investigated. The DSSC utilizing the sample with 0.3 M thiourea demonstrates the highest power conversion efficiency, η of 1.80% due to the highest dye loading, the lowest bulk and charge transfer resistance and the longest carrier lifetime. Combining TiO_2 with sulphur in composite structure was found as an effective way of enhancing the efficiency of the DSSC.*

Keywords: Dye-sensitized solar cells, photoanode, TiO_2-sulphur composite

1. INTRODUCTION

Photoanode in dye-sensitized solar cell (DSSC) serves a medium for light absorption mainly in visible region and transfer the generated charge carriers to transparent conducting oxide (TCO). Several approaches have been attempted to tune the properties of TiO_2 such as doping with other elemental ions, development of nanocomposites and synthesis of new nanostructures to enhance the performance of DSSC [1]. Improving the optical and electrical properties lead to the enhancement of the performance parameters of the device such as photocurrent and power conversion efficiency. The modifications include coating TiO_2 films with other metal oxide films such as ZnO [2], SnO_2 [3] and ZrO_2 [4,5]. TiO_2 was also prepared in the form of composite structure with another metal oxide such as TiO_2-ZnO [6], TiO_2-SnO_2 [7] and TiO_2-SiO_2 [8]. It can also be prepared in the form of core-shell structure such as SnO_2/TiO_2 and TiO_2/ZnO, respectively [9,10]. Zinc doped TiO_2 has been employed as photoanode of DSSC and demonstrated the efficiency of 1.34% [11]. Germanium doped TiO_2 has been utilized in the device in order to enhance electron transfer and power conversion efficiency [12]. TiO_2-diamond nanocomposite has been utilized as photoanode of the device [13]. The short-circuit current density and efficiency was found to be improved significantly via these photoanode modifications.

This work is concerned with the modification of TiO_2 by combining it with sulphur in composite form. The new idea of this work is the use of TiO_2-sulphur composite as a photoanode of the DSSC. So far, there has been no report on the use of TiO_2-nonmetal films composite as photoanode of the device. The goal of this work is to investigate the influence thiourea concentration on the structural and optical properties of TiO_2-sulphur composite. The second goal is to study the effect of the sulphur precursor concentration on the performance parameter of the device especially photocurrent and power conversion efficiency.

2. EXPERIMENTAL

2.1. TiO_2-sulphur composite preparation

TiO_2 films were grown on indium tin oxide (ITO) substrate by liquid phase deposition method. Firstly, ITO substrate purchased from Kaivo China with a sheet resistance of 16 Ω/square was cleaned in an ultrasonic bath using acetone and 2-propanol in a right sequence. Next, the cleaned ITO was immersed into a growth solution consisting of 7 mL of $(NH_4)_2TiF_6$ (Sigma Aldrich) and H_3BO_3 (Sigma Aldrich) with the molarity of 1.0 M and 2.0 M, respectively for 15 hours. The TiO_2 film was annealed at 400 °C for 1 hour in air. The as-prepared TiO_2 sample was then spin coated with 0.10 M thiourea (CH_4N_2S). This step was repeated with 0.30, 0.5, 1.0 and 2.0 M thiourea. The source of sulphur was thiou-

*To whom correspondence should be addressed: Email: mohd.yusri@ukm.edu.my
Phone: +60389118543; Fax: +60389250439

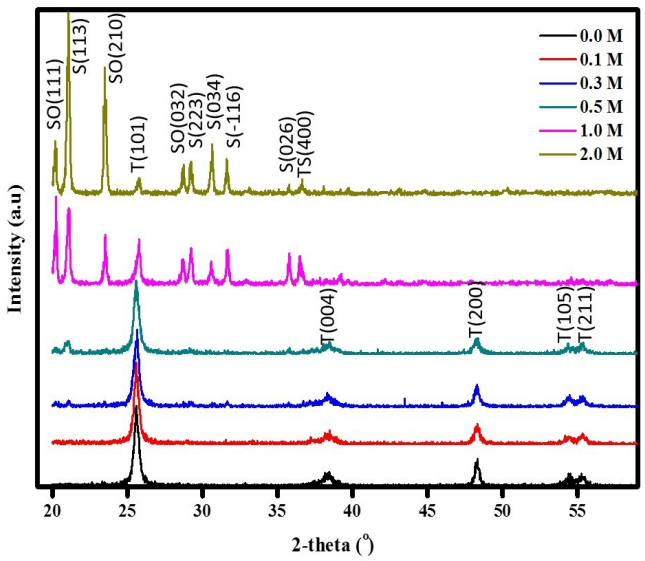

Figure 1. XRD spectra of TiO_2-sulphur composite films with various CH_4N_2S concentrations

rea which was purchased from Sigma Aldrich. The preparation of TiO_2-sulphur composite samples was completed by rinsing the sample with adequate amount of deionized water to remove the agglomerated particles on the surface of the sample and underwent annealing process in air at 100 °C for 1 hour.

The phase structure of the samples was characterized using X-ray diffraction (XRD) measurements (Bruker D8 Advance system). The optical properties characterization were carried by using UV–Vis spectrophotometer in diffused reflectance mode (DR) (Hitachi U-3900H) and photoluminescence spectroscopy by using Edinburgh Instrument FLSP920 spectrophotometer. The excitation wavelength was 300 nm. In order to obtain more information about the structure of TiO_2-sulphur composite, Raman analysis at room temperature has been carried out.

2.2. Fabrication and performance study of the DSSC

All TiO_2-sulphur composite samples were sensitized with N719 dye by immersing the samples in N719 dye (Solaronix) at temperature of 60 °C for 5 hours. Platinum film with thickness of 20 mm sputtered on the ITO substrate serves as a counter electrode. A DSSC was fabricated by sandwiching a surlyn film between TiO_2-sulphur composite and platinum counter electrode and clamped in order to optimize the interfacial contact between the TiO_2- sulphur/dye/electrolyte and the electrolyte/platinum. The Z-50 electrolyte from solaronix was injected into the space between TiO_2-sulphur/dye and platinum via a capillary action. The surlyn film serves as a separator and electrolyte container. The performance study of the device utilizing the TiO_2-sulphur composite with various thiourea concentrations was carried out by observing the current–voltage under illumination using an AM 1.5 simulated light with an intensity of 100 mW cm^{-2}. The active area of the device was 0.23 cm^2. The current–voltage curves and impedance spectra under illumination were recorded by a Gamry measurement system interfaced with a personal computer.

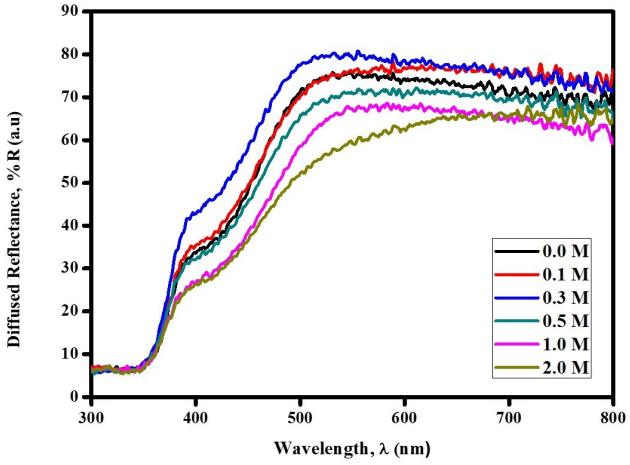

Figure 2. UV-Vis reflection spectra of TiO_2-sulfur composite films with various CH_4N_2S concentrations

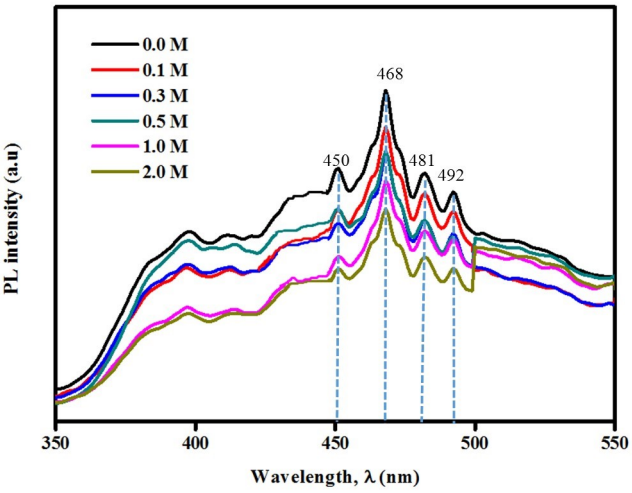

Figure 3. PL spectra of TiO_2-sulfur composite films with various CH_4N_2S concentrations

3. RESULTS AND DISCUSSION

Fig. 2 illustrates the diffused reflection spectra (DRS) for all samples. The sample with 0.3 M CH_4N_2S possesses the highest diffused reflection (80%) in the wavelength range of 500-550 nm which is in the visible region. This indicates that this sample has the best scattering light ability in the visible region. In the infrared region, the samples with the concentration of 0.1 and 0.3 M have the highest scattering property. Good scattering property tells that the film has high light harvesting efficiency when incorporating with sensitizer resulting in higher photocurrent when applied in DSSC, consequently improves the power conversion efficiency [17]. The 2.0 M sample has the lowest reflection in the visible region (63%). In other words, the DSSC utilizing the 0.3 M sample has the highest light harvesting efficiency and expected to demonstrate the highest photocurrent and power conversion efficiency.

Fig. 3 depicts the photoluminescence spectra for all samples. Basically, there two factors that influence the photoemission: i)

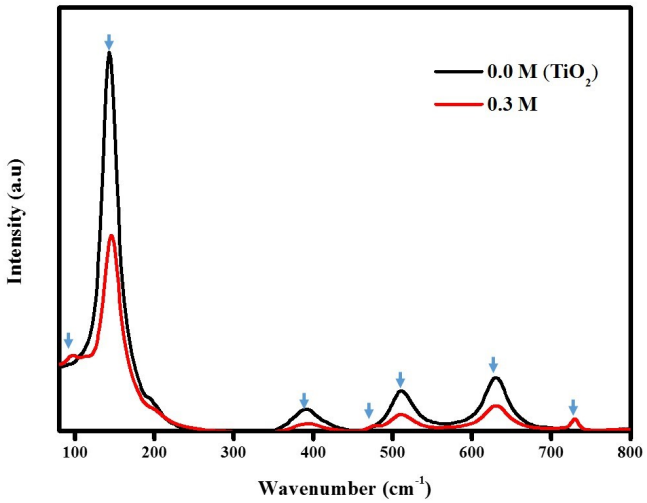

Figure 4. Raman spectra of bare TiO_2 and TiO_2-sulfur composite films with 0.3 M CH_4N_2S

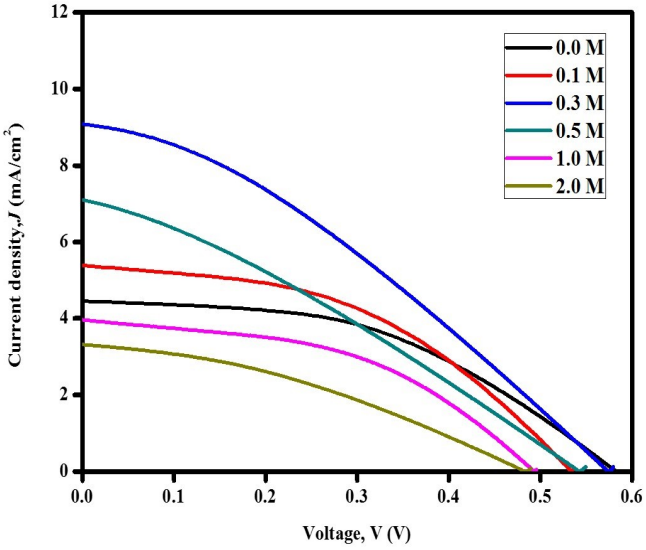

Figure 5. *J-V* curves of the devices utilizing TiO_2-sulphur composite films with various CH_4N_2S concentrations

excitation emission, contributed by transition of electron from conduction band to valence band and ii) defect emission, resulted from transition of electron from defect energy level to valence band. Since TiO_2 is the host of the composite system in this work, the photoemission peaks might be attributed from TiO_2 characteristics. The sub-band of 388 nm contributed by the excitation emission was not observed because anatase TiO_2 is an indirect bandgap material, and most PL observed was attributed from the transitions of defects in TiO_2 [18]. The band emission at 450, 468 and 481 nm in blue regions are due to different intrinsic defects of TiO_2 such as neutral oxygen vacancy, cation vacancy and interstitial defect [19, 20]. The emissions at those wavelengths are exhibited from the transition of electron from energy level of previous mentioned defects to the valence band. A green emission observed at 492 nm is due to the donor–acceptor recombination or charge transitions from the conduction band to oxygen vacancies [21]. The increase of sulphur content in the preparation process of TiO_2-sulphur composite samples may play a major role and modifies the intensity of photoemission. However, the peak position is not sensitive to the change in sulphur content but the emission intensity is decreased with the sulphur content, considerably due to the inclusion of sulphur in TiO_2. This PL quenching suggests that the recombination process decreases with the increase of sulphur content. The decrease of recombination process increases the electron density.

Fig. 4 displays the Raman spectrum of TiO_2 and TiO_2-sulphur nanocomposite (0.3 M) excited with a 514.5 nm beam of the Ar+ laser. Group theory predicts that the typical anatase TiO_2 has six Raman active modes: $\Gamma = A_{1g} + 2B_{1g} + 3_{Eg}$. For TiO_2, the Raman spectra present four bands at 144 cm^{-1} (E_g), 390 cm^{-1} (B_{1g}), 507 cm^{-1} (A_{1g}) and 628 cm^{-1} (E_g). All samples that exhibit the characteristic Raman-active modes of the anatase TiO_2 phase are in good agreement with the phase structure determined by XRD [22]. For TiO_2-sulphur composite with sulphur precursor concentration of 0.3 M, a small peak at 474 cm^{-1} corresponds to the A_{1g} symmetric stretching mode of S [23,24]. Other bands that present in the spectra might be from the complex compound of TiO_2-sulphur composite system.

Fig. 5 depicts the *J-V* curves of the DSSC employing the samples with various thiourea concentrations. It is found that the area under curves representing the output power generated by the device varies with the concentration of thiourea. The 0.3 M device generates the highest output power, while the 2.0 M device produces the lowest output power. It is also noticeable that the slope of each curve is quite high, signifying the high internal resistance in the devices.

Table 1. Crystallite size of anatase and sulphur phases with various thiourea concentrations

Concentration (M)	Crystallite size (nm)	
	Anatase (101 plane)	Sulphur (113 plane)
0.0	24.1	-
0.1	24.1	48.1
0.3	23.1	48.3
0.5	22.8	49.1
1.0	40.5	50.2
2.0	65.4	51.8

Table 2. Photovoltaic parameters and dye loading of the DSSC with various thiourea concentrations

Concentration (M)	J_{sc} (mA/cm^2)	V_{oc} (V)	η (%)	*FF*	Dye loading (mol/cm^2)
0.0	4.45±0.17	0.58±0.06	1.20±0.30	0.46±0.01	7.39
0.1	5.39± 0.03	0.58±0.06	1.31±0.11	0.42±0.03	8.23
0.3	9.08± 0.11	0.57±0.08	1.80±0.23	0.34±0.04	8.69
0.5	7.11± 0.16	0.54±0.08	1.16±0.16	0.30±0.06	7.21
1.0	3.98±0.20	0.49±0.07	0.90±0.01	0.46±0.01	6.54
2.0	3.32±0.14	0.48±0.04	0.57±0.01	0.35±0.05	5.30

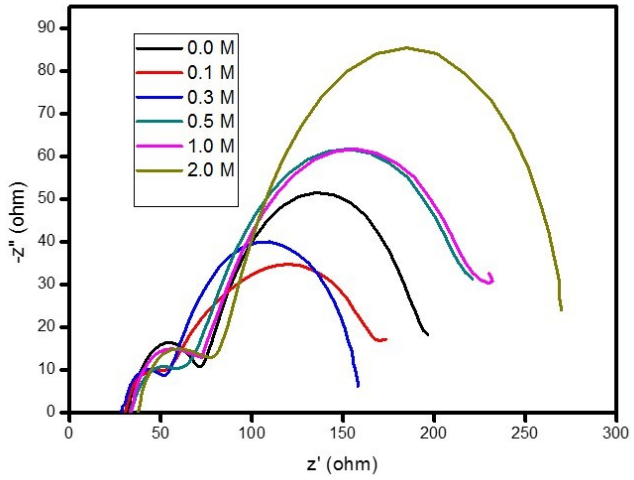

Figure 6. Nyquist plots of the devices with various CH_4N_2S concentrations

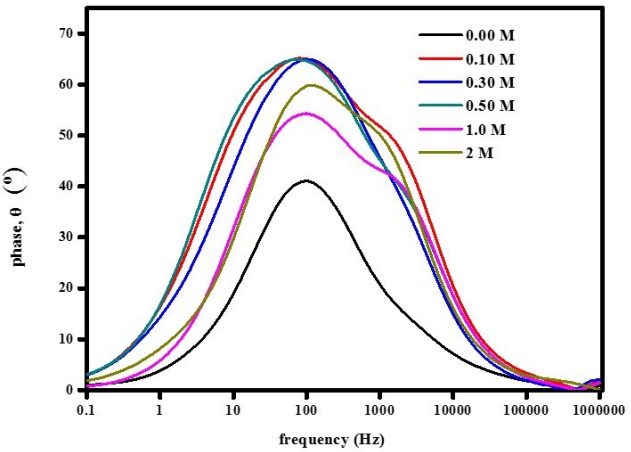

Figure 7. Bode plots of the devices with various CH_4N_2S concentrations

The photovoltaic parameters are extracted from the curves and presented in Table 2. According to the table, the J_{sc} and η increases with thiourea concentration until the optimum concentration of 0.3 M and then drops. The 0.3 M device performs the highest J_{sc} and η which is due to the highest dye loading, the lowest R_b and R_{ct} and the longest carrier lifetime. Also from the table, it is observed that the η increases with dye loading. The higher dye loading results in the higher η. The 2.0 M device demonstrates the lowest J_{sc} and η. It is also noticeable that the device utilizing the pure TiO_2 photoanode performs higher J_{sc} than that of 1.0 and 2.0 M devices. The SO_3 and Ti_3S_4 phases lower down the efficiency since according to Table 1, the η of the device utilizing 1.0 and 2.0 M samples are smaller than that of the devices with lower concentrations of thiourea. These two phases exist in the samples with 1.0 and 2.0 M thiourea as observed in the XRD patterns illustrated in Fig. 1. The device utilizing pure TiO_2 also demonstrates higher η than the 0.5, 1.0 and 2.0 M devices. Also, it is observed from the table that the efficiency of the device without sulphur (1.20%) has been improved quite significantly upon combining it with sulphur in composite form. The efficiency has been improved by 50% by modifying TiO_2 films photoanode via sulphur treatment. The highest efficiency of 1.80% was found to be higher than that reported in [10], yielding the efficiency of 0.18% only. This indicates that the highest efficiency obtained from this work is 10 times than reported in this literature. Also, from the table, the *FF* is low since the internal resistance of the devices is high leading high power loss. The V_{oc} presented in the table is also low. Low *FF* and V_{oc} lead to low efficiency of the device.

Fig. 6 shows the Nyquist plots of the devices utilizing the photoanodes with various thiourea concentrations. The plots display two semicircles for which a smaller semicircle represents bulk resistance and a bigger one denotes charge transfer resistance. From the plots, it is found that the 0.3 M device shows the smallest semicircles meanwhile the biggest semicircles belong to the 2.0 M device. Both resistances are illustrated in Table 3. Fig. 7 depicts the Bode plots for all devices. The plots are symmetry about a resonant frequency which was used to compute the carrier lifetime. The 0.3 M device has the smallest frequency leading to the highest lifetime. While, the 2.0 M device has the biggest frequency resulting in the shortest lifetime. The improved lifetime of carriers might be due to this reason. The composite sample should be subjected to annealing treatment at high temperature to remove all the organics residues and complexes in order to make sure that the samples is pure TiO_2-sulphur without the existence of any secondary phase. According to Table 3, the 1.0 and 2.0 samples have shorter carrier lifetime compared with the samples prepared using lower concentrations of thiourea.

Table 3. Parameters of the DSSC with various thiourea concentrations

Concentration (M)	R_b (Ω)	R_{ct} (Ω)	τ (ms)
0.0	39±3	122±10	6.5±0.1
0.10	38±1	120±8	6.5±0.1
0.30	38±3	118±9	7.7±0.4
0.5	40±2	131±5	7.1±0.5
1.0	42±1	180±1	6.3±0.2
2.0	42±1	210±3	5.1±0.1

4. CONCLUSIONS

TiO_2-sulphur composite films have been prepared via liquid phase deposition assisted with spin coating technique and employed as photoanode in DSSC. Apart from anatase and sulphur phases, the secondary phase of SO_3 and Ti_3S_4 also exist in the sample. The 0.3 M sample shows the highest reflection in visible region. The peak intensity at 460 nm decreases with thiourea concentration. The luminescence peak intensity in the visible region, 400-500 nm decreases with thiourea concentration. The Raman peak at 474 cm^{-1} corresponds to the A_{1g} symmetric stretching mode of sulphur. The efficiency has been improved by 50% by modifying TiO_2 films photoanode with sulphur in composite form. The DSSC utilizing this composite demonstrates the highest power conversion efficiency, η of 1.80% due to the highest dye loading, the lowest bulk and charge transfer resistance and the longest carrier lifetime.

5. ACKNOWLEDGEMENTS

The authors would like to thank Universiti Kebangsaan Malaysia for providing a financial support through a research grant GUP-2016-013.

REFERENCES

[1] M.S. Ahmad, A.K. Pandey, N.A. Rahim, A review. Renew. Sustain. Energy Rev., 77, 89 (2017).
[2] C. Xu, J. Wu, U. V. Desai, D. Gao, Nano Lett., 12, 2420 (2012).
[3] J. Qian, P. Liu, Y. Xiao, Y. Jiang, Y. Cao, X. Ai, H. Yang, Adv. Mater. 21, 3663 (2009).
[4] T.C. Li, M.S. Góes, F. Fabregat-Santiago, J. Bisquert, P.R. Bueno, C. Prasittichai, J.T. Hupp, T.J. Marks, J. Phys. Chem. C, 113, 18385 (2009).
[5] D.B. Menzies, R. Cervini, Y.-B. Cheng, G.P. Simon, L. Spiccia, J. Sol-Gel Sci. Technol., 32, 363 (2004).
[6] N. Rajkumar, S.S. Kanmani, K. Ramachandran, Adv. Sci. Lett., 4, 627 (2011).
[7] C. Wang, I-C. Cheng, J-Z. Chen, ECS J. Solid State Sci. Technol., 4, 3020 (2015).
[8] X. Wang, M. Xi, H. Fong, Z. Zhu, ACS Appl. Mater.Interfaces, 6, 15925 (2014).
[9] C. Gao, X. Li, B. Lu, L. Chen, Y. Wang, F. Teng, J. Wang, Z. Zhang, X. Pan, E. Xie, Nanoscale, 4, 3475 (2012).
[10] S.S. Kanmani, K. Ramachandran, Renewable Energy, 43, 149 (2012).
[11] M.S. Ahmad, A.K. Pandey, N.A. Rahim, Mater. Lett. 195, 62 (2017).
[12] M.S. Ahmad, A.K. Pandey, N.A. Rahim, Optik 157, 134 (2018).
[13] S. Ahmad, A.K. Pandey, N.A. Rahim, Arabian J. Sci. Eng. 2017 (DOI: 10.1007/s13369-017-2979-z).
[14] X.Z. Ma, B. Jin, H.Y. Wang, J.Z. Hou, X.B. Zhong, H.H. Wang, P.M. Xin, J. Electroanal. Chem., 736, 127 (2015).
[15] K. Xie Y. Han, W. Wei, H. Yu, C. Zhang, J-G. Wang, W. Lu, B. Wei, RSC Adv. 5, 77348 (2015).
[16] X. Chen, S.S. Mao, Chem. Reviews, 107, 2891 (2007).
[17] V. Dhas, S. Muduli, S. Agarkar, A. Rana, B. Hannoyer, R. Banerjee, S. Ogale, Solar Energy, 85, 1213 (2011).
[18] Y-H. Chang, C-M. Liu, C. Chen, H-E. Cheng, J. Electrochem. Society, 159, 401 (2012).
[19] A.S. Ganeshraja, K. Rajkumar, K. Zhu, X. Li, S. Thirumurugan, W. Xu, J. Zhang, M. Yang, K. Anbalagan, J. Wang, RSC Adv. 6, 72791 (2016).
[20] S. Majumder, S.K. Jana, K. Bagani, Optical Mater., 40, 97 (2015).
[21] X. Wang, Z. Feng, J. Shi, G. Jia, S. Shen, J. Zhou, C. Li, Phys. Chem. Chem. Phys., 12, 7083 (2012).
[22] J. Shen, H. Wang, Y. Zhou, N. Ye , G. Li, L. Wang, RSC Adv. 2, 9173 (2012).
[23] A.T. Ward, J. Phys. Chem., 72, 4133 (1968).
[24] A. J. Blake, K. Dorney, I.E. Sizemore, H. Huang, J. Nanomater., 9, (2015) Article ID 212938.